



Biosupercapacitors Hot Paper

How to cite: *Angew. Chem. Int. Ed.* **2021**, *60*, 10563–10567

International Edition: doi.org/10.1002/anie.202101388

German Edition: doi.org/10.1002/ange.202101388

Implantable Biosupercapacitor Inspired by the Cellular Redox System

Yongwoo Jang⁺, Taegyu Park⁺, Eunyung Kim, Jong Woo Park, Dong Yeop Lee, and Seon Jeong Kim*

Abstract: The carbon nanotube (CNT) yarn supercapacitor has high potential for *in vivo* energy storage because it can be used in aqueous environments and stitched to inner parts of the body, such as blood vessels. The biocompatibility issue for frequently used pseudocapacitive materials, such as metal oxides, is controversial in the human body. Here, we report an implantable CNT yarn supercapacitor inspired by the cellular redox system. In all living cells, nicotinamide adenine dinucleotide (NAD) is a key redox biomolecule responsible for cellular energy transduction to produce adenosine triphosphate (ATP). Based on this redox system, CNT yarn electrodes were fabricated by inserting a twist in CNT sheets with electrochemically deposited NAD and benzoquinone for redox shuttling. Consequently, the NAD/BQ/CNT yarn electrodes exhibited the maximum area capacitance (55.73 mFcm^{-2}) under physiological conditions, such as phosphate-buffered saline and serum. In addition, the yarn electrodes showed a negligible loss of capacitance after 10000 repeated charge/discharge cycles and deformation tests (bending/knotting). More importantly, NAD/BQ/CNT yarn electrodes implanted into the abdominal cavity of a rat's skin exhibited the stable *in vivo* electrical performance of a supercapacitor. Therefore, these findings demonstrate a redox biomolecule-applied platform for implantable energy storage devices.

The recent development of wearable electronic devices enables a platform for monitoring diverse surroundings and physiological signals on the body.^[1] In step with this growth, flexible and stretchable supercapacitors have been developed to maintain stable performance and safety.^[2] For implantable electronics, further considerations, such as reliable compatibility and stability in biological fluids, are needed in current supercapacitors. To improve intrinsic capacitance, transition metal oxides, such as MnO_2 and NiO_2 , have been frequently used as a pseudocapacitive material.^[3] Although these metal oxides are highly attractive as supercapacitors, they still have a disadvantage in applications in implantable electronics due to their poor biocompatibility.^[4]

To overcome this biocompatibility issue, several studies have attempted to apply biomolecules to a supercapacitor to improve its performance. For example, Hur and colleagues

described a DNA-based supercapacitor that was fabricated from a poly(3,4-ethylenedioxythiophene):poly(styrenesulfonate) (PEDOT:PSS)-coated DNA hydrogel on gold foil.^[5] The DNA-based supercapacitor showed capacitive performance in biological fluids, such as artificial urine and phosphate buffered saline (PBS). More recently, Sim et al. utilized a ferritin protein as a guest as a supercapacitor. The ferritin-composite supercapacitor was bisrolled with PEDOT:PSS in the CNT (carbon nanotube) yarn, which exhibited the electrical performance of a supercapacitor in PBS and after *in vivo* implantation into the abdominal cavity of a mouse.^[6] These supercapacitors are mainly based on charged biomolecules, such as DNA and ferritin, to increase their intrinsic capacitance.^[7] In the current study, we undertook the challenge of applying redox-mediated biomolecules as a pseudocapacitive material, such as metal oxides for a redox supercapacitor.

In cellular energy transduction, nicotinamide adenine dinucleotide (NAD) is an essential cofactor and is an electron carrier in redox reactions.^[8] In general, NAD^+ is reduced to NADH during glycolysis in the cytoplasm, and cytosolic NADH is oxidized by transferring electrons to the electron transport chain of mitochondria.^[8] The conversion of NAD^+ to NADH is reversibly regulated by a certain specific enzyme without a net loss of NAD.^[8] Consequently, redox shuttling of NAD is critical to generate adenosine triphosphate (ATP) in energy production in all living cells.^[9] In fact, NAD-dependent enzymes, such as NAD-dependent glucose dehydrogenase and malate dehydrogenase, have been employed as anodes for oxidation in enzymatic biofuel cells.^[10] As an enzyme-independent mechanism, benzoquinones (BQs) have been known to facilitate the oxidation of NADH from 0.0745 to $9220 \text{ M}^{-1} \text{ s}^{-1}$.^[11]

In the present study, we describe a flexible biosupercapacitor fiber based on the redox system of NAD for implantable devices. The yarn electrodes for the biosupercapacitor are fabricated by a bisrolling process inserting a twist in a host CNT sheet that is overlaid with NAD^+ and benzoquinone as guests. The areal capacitance of the biosupercapacitor is 55.73 mFcm^{-2} in PBS. The areal energy density and power density are $19.81 \mu\text{Whcm}^{-2}$ and 446 Wcm^{-2} , respectively, which are approximately 27.5 times higher than those of the guest-free CNT yarn. When operated in the abdominal cavity of rats, the implanted biosupercapacitor exhibit electrochemical performances similar to the *in vitro* results in PBS.

The fabrication of NAD/BQ/CNT yarn electrodes is illustrated in Figure 1 A. The yarn bisrolled from the CNT sheet serves as a current collector and a host material. To improve the intrinsic capacitance in biological conditions, a redox molecule, NAD^+ was used as a guest material. In redox reactions, the reduction of two electrons and a proton

[*] Y. Jang,^[†] T. Park,^[†] E. Kim, J. W. Park, D. Y. Lee, Prof. S. J. Kim
Center for Self-powered Actuation and Department of Biomedical
Engineering, Hanyang University
Seoul 04736 (Korea)
E-mail: sjk@hanyang.ac.kr

[†] These authors contributed equally to this work.

Supporting information and the ORCID identification number(s) for the author(s) of this article can be found under:
<https://doi.org/10.1002/anie.202101388>.

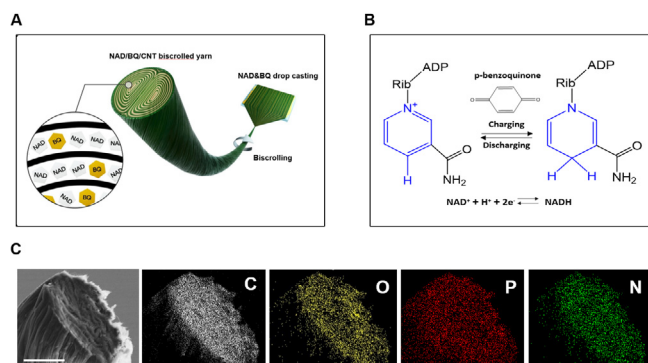


Figure 1. A) Fabrication Scheme and images of the NAD/BQ/CNT yarn supercapacitor. B) Molecular structure of nicotinamide adenine dinucleotide (oxidized and reduced forms abbreviated as NAD^+ and NADH , respectively). C) SEM image and elemental mapping analysis performed on the cross-section area; the locations of C (carbon, white dot), O (oxygen, yellow dot), N (nitrogen, green dot), and P (phosphorus, red dot) are spotted. (The scale bar indicates $50\ \mu\text{m}$).

to the nicotinamide moiety of NAD^+ produces NADH , as shown in Figure 1B. To catalyze the redox shuffling of NAD and NADH , we also used BQ, which has a single benzene ring. First, BQ was dispersed by sonication in an ethanol solution, which was dropped onto CNT sheets drawn from a carbon multiwalled nanotube forest. Ethanol increased the density of the CNT nanofibers. After evaporating the ethanol solution, NAD^+ was dropped onto the BQ-contained CNT sheet. Subsequently, the NAD/BQ-coated CNT sheet was twisted at 1000 turns per meter of the initial sheet length to form a bisrolled yarn. Furthermore, the NAD/BQ-coated CNT yarn was coated with Nafion to prevent the loss of material in the charge-discharge cycle.

Figure 1C shows a cross-section SEM image and an EDS mapping image of the 85 wt % NAD/BQ/CNT fiber. The EDS mapping image represents the distribution of C (white), O (yellow), P (red), and N (green) atoms that NAD^+ is composed of in the CNT yarn (Figure 1C). The EDS analysis shown in Figure S1 presents the presence of C, O, N and P atoms in the electrode, which indicates the composition of NAD^+ .

The electrochemical performance of a NAD/BQ/CNT electrode was measured with a three-electrode system in 1 M KCl electrolyte. The area capacitance was normalized by the total external surface area of a single electrode. As shown in Figure 2A, the measurement of the cyclic voltammetry (CV) of a pristine CNT showed the rectangular dependence of the current density on the applied potential, which is consistent with the energy storage by the electrochemical double-layer charge capacitance of the CNTs ($2\ \text{mF cm}^{-2}$). The current density of the bare CNT yarn was increased by the addition of BQ ($23.6\ \text{mF cm}^{-2}$). In fact, several quinone derivatives have been shown to enhance the capacitive performance of carbon electrodes.^[12] Remarkably, the NAD/BQ/CNT electrode exhibited a robust increase in capacitance at an applied potential compared with a bare CNT and BQ/CNT, which corresponds to the redox reaction of NAD^+ and NAD because BQ facilitates the oxidation of NADH . Figure 2B indicates the difference of capacitance between 10 wt % and

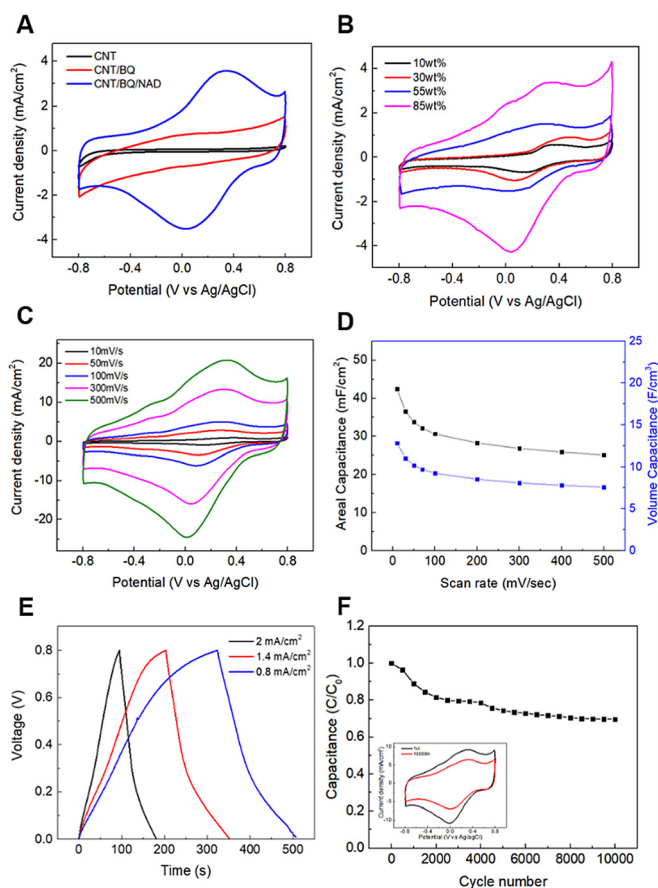


Figure 2. A) Comparison of the CV curves (at $100\ \text{mV s}^{-1}$) of pristine CNT yarn (black line), BQ/CNT composite yarn (red line) and NAD/BQ/CNT composite yarn supercapacitors (blue line). B) CV curves of 10 wt %, 30 wt %, 55 wt % and 85 wt % of the NAD/BQ/CNT yarn supercapacitor. C) CV curves measured from 10 to $500\ \text{mV s}^{-1}$ for the NAD/BQ/CNT yarn supercapacitor. D) Areal capacitance and volume capacitance of the NAD/BQ/CNT yarn supercapacitor. E) Galvanostatic charge/discharge curves (measured from 0.8 to $2\ \text{mA cm}^{-2}$) of the NAD/BQ/CNT yarn supercapacitor. F) Capacitance retention of the supercapacitor during charge/discharge cycles. The inset graph compares CV curves before and after 10000 charge/discharge cycles.

85 wt % NAD/BQ (10:1 weight ratio of $\text{NAD}:\text{BQ}$). Among those, it revealed that 85 wt % NAD/BQ in CNT yarn exhibits the highest areal capacitance ($52.22\ \text{mF cm}^{-2}$).

For comparing the CV graphs of the NAD/BQ/CNT electrode at different scan rates, Figure 2C shows the CV graph with scan rate from $10\ \text{mV s}^{-1}$ to $500\ \text{mV s}^{-1}$. The reduction peak is formed at approximately $0.3\ \text{V}$, and the oxidation peak is formed at approximately $0.1\ \text{V}$. Figure 2D shows the capacitance retention when the scan rate changes from $10\ \text{mV s}^{-1}$ to $500\ \text{mV s}^{-1}$. The highest capacitance values per area and volume when the scan rate is $10\ \text{mV s}^{-1}$ are $55.73\ \text{mF cm}^{-2}$ $16.57\ \text{mF cm}^{-3}$, respectively. In addition, the NAD/BQ/CNT electrode shows an electrochemically stable value of 60 % retention at a $500\ \text{mV s}^{-1}$ scan rate. Figure 2E shows the galvanostatic charge/discharge curves measured from current densities of 0.8 to $2\ \text{mA cm}^{-2}$. The highest capacitance is $52.5\ \text{mF cm}^{-2}$ at $0.8\ \text{mA cm}^{-2}$, and the triangular charge/discharge patterns are consistent with energy storage

by the electrochemical double-layer charging capacitance of the CNT and the pseudocapacitance materials. In addition, the Nyquist curve of the NAD/BQ/CNT yarn supercapacitor has a typical supercapacitor shape with a $33.58 \Omega \text{ cm}^{-1}$ initial equivalent series resistance (ESR) (Figure S2). Therefore, it seems that NAD is involved in the pseudocapacitance of the NAD/BQ/CNT yarn supercapacitor. The capacitance retention during repeated charge-discharge cycles is shown in Figure 2F. The capacitance retention test was measured for 10000 cycles at a scan rate of 100 mVs^{-1} . The NAD/BQ/CNT yarn supercapacitor exhibits approximately 88.98% and 69.61% capacitance retention for 1000 and 10000 cycles, respectively.

To determine its potential for use as implantable electronic device, the performance of the NAD/BQ/CNT yarn supercapacitor was evaluated in phosphate buffered saline (PBS), Hank's balanced salt solution (HBSS), and serum, which are frequently used as models of biological fluids. As shown in Figure 3A, the CV measurement of the NAD/BQ/CNT yarn showed a similar rectangular dependence of the CV graph on the applied potential in several simulated body fluids. At 10 mVs^{-1} , the performance values of the supercapacitor were 23.31 mF cm^{-2} (PBS), 26.31 mF cm^{-2} (saline), 32.35 mF cm^{-2} (HBSS), and 33.15 mF cm^{-2} (serum). In addition, Figure 3B shows the capacitance retention when the scan rate changed from 10 to 500 mVs^{-1} in the above solutions. The NAD/BQ/CNT yarn supercapacitor showed an electrochemically stable value of 55% retention at a scan rate of 500 mVs^{-1} . Similar to the KCl electrolyte, the NAD/BQ/CNT yarn supercapacitor showed a Nyquist curve with a $96 \Omega \text{ cm}^{-1}$ initial ESR (Figure 3C) and a 92% capacitance

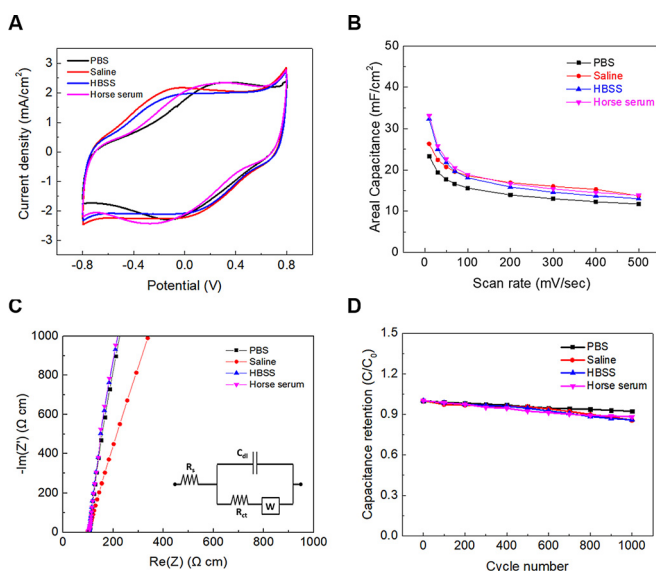


Figure 3. A) CV curves of the symmetric NAD/BQ/CNT supercapacitor at 10 mVs^{-1} in PBS, saline, HBSS, and serum. B) Areal capacitance of the NAD/BQ/CNT yarn supercapacitor in PBS, saline, HBSS, and serum. C) A Nyquist curve with a $96 \Omega \text{ cm}^{-1}$ initial ESR of the NAD/BQ/CNT yarn supercapacitor. The inset is the equivalent circuit of Randle's model. D) Capacitance retention of the supercapacitor during 1000 charge/discharge cycles measured in PBS, saline, HBSS, and serum.

retention for 1000 cycles at a scan rate of 100 mVs^{-1} (Figure 3D).

Implementing this supercapacitor requires an energy storage system that is flexible and resistant to mechanical damage under physiological conditions. To confirm this, we measured the electrochemical performance of the supercapacitor during mechanical deformations. Remarkably, the capacitance retention (Figure 4A) and the CV curves (Figure 4B) of the NAD/BQ/CNT yarn were stably maintained without loss during 1000 bending cycles. Even with a knot, the current density of the supercapacitor was well maintained without a break (Figure 4C). Figure 4D indicates the mechanical property of our yarn electrode. Its tensile strength is measured at 153 MPa, which seems that has sufficient strength compared to frequently used suture fibers including in polylactic acid, polycaprolactone.^[13] To demonstrate the performance and applicability of our supercapacitor, we attempted to connect to a light-emitting diode (LED). Consequently, the LED light was lighted when two yarn electrodes were connected in series (Figure 4E). Therefore,

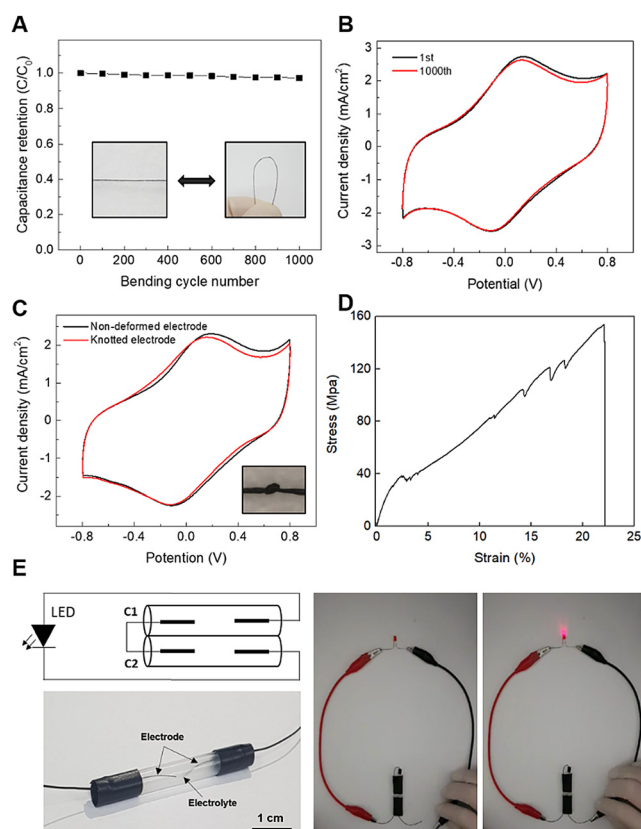


Figure 4. A) Capacitance retention depending on bending cycles. The inset presents optical images of the NAD/BQ/CNT supercapacitor with/without bending deformation. B) CV curves of the NAD/BQ/CNT yarn supercapacitor at the 1st and 1000th bending. C) CV curves of the NAD/BQ/CNT yarn supercapacitor in non-deformed (black) and deformed (red) states. The inset shows an optical image of the NAD/BQ/CNT supercapacitor with knotted deformation. D) Stress-strain curve of the NAD/BQ/CNT yarn. E) Circuit diagram and optical image of symmetric NAD/BA/CNT supercapacitor (left). A red-light emitting diode (LED) powered by symmetric NAD/BQ/CNT supercapacitor in series (right).

the NAD/BQ/CNT yarn supercapacitor has reliable compatibility and stability even for mechanical deformations in biological fluids.

More importantly, we further examined the *in vivo* performance of the NAD/BQ/CNT yarn supercapacitor in rats. Animal care and handling was carried out according to guidelines issued by Hanyang University's Institutional Animal Care and Use Committee and followed National Institutes of Health guidelines. The two flexible yarn electrodes were sutured in parallel into the abdominal cavity of rats, as shown in the Figure 5 A. The implanted supercapacitor in the subcutaneous tissue of rats effectively exhibited a similar electrochemical performance to that in PBS (Figure 5 B). The galvanostatic charge/discharge curve at 2.66 mA cm^{-2} showed a typical triangular charge/discharge graph, which indicates that the NAD/BQ/CNT yarn electrode effectively functions as a supercapacitor *in vivo* (Figure 5 C). The performance of our supercapacitor implanted in three different rats was monitored over two weeks. The capacitance values on the day of implantation were retained at approximately 86.9% two weeks later (Figure 5 D), and it also exhibited approximately 11% capacitance retention after 1000 cycles in the rats

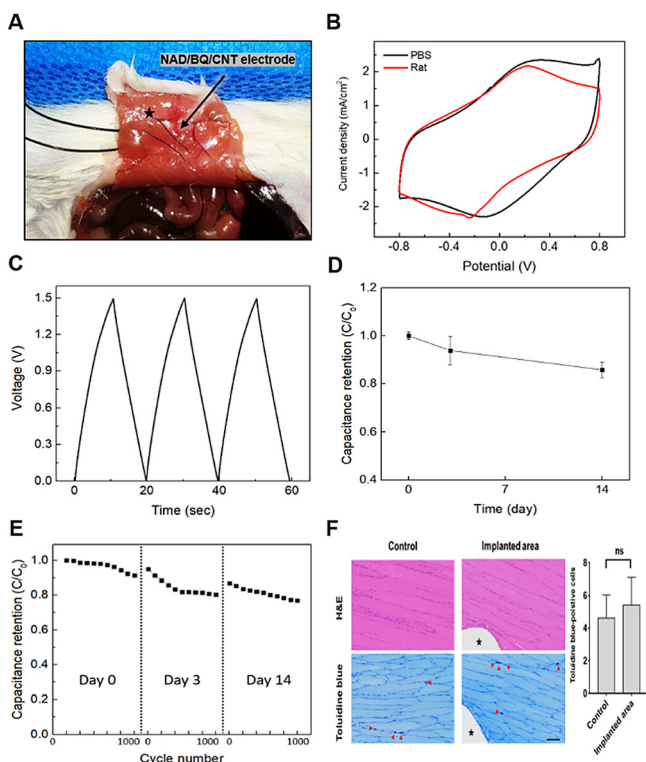


Figure 5. A) Photograph of the NAD/BQ/CNT yarn supercapacitor implanted into the abdominal cavity of a rat. B) Comparison of the CV graphs of the performance of the NAD supercapacitor in PBS and implanted in a rat. C) Galvanostatic charge-discharge curves measured at 2.66 mA cm^{-2} of the NAD/BQ/CNT yarn supercapacitor. D) Changes in capacitance over time after implantation. E) Capacitance retention of the supercapacitor after each 1000 charge/discharge cycles. The capacitance retention was measured at the day of surgery, 3 and 14 days after implantation. F) Histological analysis by H&E and toluidine blue staining in control and implanted tissues. Scale bar indicates $100 \mu\text{m}$.

(Figure 5 E). These results suggest high capacitance stability *in vivo* circumstance. Furthermore, we examined the biocompatibility of our supercapacitor 2 weeks after implantation. To investigate this, the abdominal tissue that was attached the yarn electrodes two weeks after implantation was stained by hematoxylin and eosin (H&E, for histology) and toluidine blue (for mast cells) methods for generally identifying immune response.^[14] In the Figure 5, star mark indicates the area where the wires were connected to measure our device, and red arrow means toluidine-positive cells. As a result, there was no notable difference in the histological analysis between H&E stained images of yarn electrodes-contained area and opposite control area. Toluidine blue is often used to identify mast cells that are a migrant immune cell of connective tissue, and the number of mast cell can represent the degree of inflammation. As shown in Figure 5 F, there was no significant difference in the toluidine-positive cells between control (4.6 ± 1.4) and implanted area (5.4 ± 1.7) in the field ($800 \mu\text{m} \times 600 \mu\text{m}$). Therefore, these findings support a remarkable biocompatibility of our NAD/BQ/CNT electrode.

In summary, the present study describes an implantable supercapacitor using NAD^+ , which is a key redox biomolecule responsible for cellular energy transduction. The NAD/BQ/CNT yarn supercapacitor showed the expected electrochemical performance in various simulated body fluids (PBS, HBSS, saline, serum) and exhibited a negligible loss of capacitance after 1000 repeated charge/discharge cycles and deformation tests (bending/knotting). The flexible yarn-type supercapacitor was easily sutured to the subcutaneous layer of a rat's skin, showing stable performance for use as a supercapacitor. Taken together, these findings establish a potential platform for an implantable supercapacitor to improve intrinsic capacitance instead of transition metal oxides.

Acknowledgements

This work was supported by the Creative Research Initiative Center for Self-powered Actuation in the National Research Foundation of Korea and the National Research Foundation of Korea grant funded by the Korea government (No.2020R1A4A1016840).

Conflict of interest

The authors declare no conflict of interest.

Keywords: carbon nanotube · nicotinamide adenine dinucleotide · supercapacitor

- [1] a) W. Zeng, L. Shu, Q. Li, S. Chen, F. Wang, X. M. Tao, *Adv. Mater.* **2014**, *26*, 5310–5336; b) M. Mardonova, Y. Choi, *Energies* **2018**, *11*, 547.
- [2] a) L. Li, Z. Lou, D. Chen, K. Jiang, W. Han, G. Shen, *Small* **2018**, *14*, 1702829; b) K. Keum, J. W. Kim, S. Y. Hong, J. G. Son, S. S. Lee, J. S. Ha, *Adv. Mater.* **2020**, *32*, 2002180; c) Y. Jang, S. M. Kim, G. M. Spinks, S. J. Kim, *Adv. Mater.* **2020**, *32*, 1902670.

- [3] a) C. Choi, J. A. Lee, A. Y. Choi, Y. T. Kim, X. Lepro, M. D. Lima, R. H. Baughman, S. J. Kim, *Adv. Mater.* **2014**, *26*, 2059–2065; b) C. Choi, K. M. Kim, K. J. Kim, X. Lepro, G. M. Spinks, R. H. Baughman, S. J. Kim, *Nat. Commun.* **2016**, *7*, 13811; c) C. Choi, J. M. Lee, S. H. Kim, S. J. Kim, J. T. Di, R. H. Baughman, *Nano Lett.* **2016**, *16*, 7677–7684.
- [4] a) H. A. Jeng, J. Swanson, *J. Environ. Sci. Health Part A* **2006**, *41*, 2699–2711; b) S. P. Singh, M. Kumari, S. I. Kumari, M. F. Rahman, M. Mahboob, P. Grover, *J. Appl. Toxicol.* **2013**, *33*, 1165–1179; c) M. Gotić, T. Jurkin, S. Musić, K. Unfried, U. Sydlik, A. Bauer-Šegvić, *J. Mol. Struct.* **2013**, *1044*, 248–254.
- [5] J. Hur, K. Im, S. Hwang, B. Choi, S. Kim, S. Hwang, N. Park, K. Kim, *Sci. Rep. UK* **2013**, *3*, 1282.
- [6] H. J. Sim, C. Choi, D. Y. Lee, H. Kim, J. H. Yun, J. M. Kim, T. M. Kang, R. Ovalle, R. H. Baughman, C. W. Kee, S. J. Kim, *Nano Energy* **2018**, *47*, 385–392.
- [7] a) H. Kim, J. W. Park, J. S. Hyeon, H. J. Sim, Y. Jang, Y. Shim, C. Huynh, R. H. Baughman, S. J. Kim, *Biosens. Bioelectron.* **2020**, *164*, 112318; b) Y. Jang, S. M. Kim, K. J. Kim, H. J. Sim, B. J. Kim, J. W. Park, R. H. Baughman, A. Ruhparwar, S. J. Kim, *ACS Sens.* **2019**, *4*, 2893–2899.
- [8] a) M. Pehar, B. A. Harlan, K. M. Killoy, M. R. Vargas, *Antioxid. Redox Signaling* **2018**, *28*, 1652–1668; b) Y. Jang, B. Lee, H. Kim, S. Jung, S. H. Lee, S. Y. Lee, J. H. Jeon, I. B. Kim, S. H. Lee, B. J. Kim, U. H. Kim, Y. Lee, S. M. Kim, D. Jeon, U. Oh, *Mol. Neurobiol.* **2019**, *56*, 3819–3832; c) P. J. Elving, W. T. Bresnahan, J. Moiroux, Z. Samec, *Bioelectrochem. Bioenerg.* **1982**, *9*, 365–378.
- [9] J. D. Rabinowitz, S. Enerback, *Nat. Metab.* **2020**, *2*, 566–571.
- [10] a) G. Wu, Y. Gao, D. Zhao, P. Ling, F. Gao, *ACS Appl. Mater. Interfaces* **2017**, *9*, 40978–40986; b) A. Nasar, R. Perveen, *Int. J. Hydrogen Energy* **2019**, *44*, 15287–15312.
- [11] a) T. Iyanagi, *Biochim. Biophys. Acta Bioenerg.* **2019**, *1860*, 233–258; b) B. W. Carlson, L. L. Miller, *J. Am. Chem. Soc.* **1985**, *107*, 479–485.
- [12] a) N. Tisawat, C. Samart, P. Jaiyong, R. A. Bryce, K. Nueangnoraj, N. Chanlek, S. Kongparakul, *Appl. Surf. Sci.* **2019**, *491*, 784–791; b) A. M. Navarro-Suárez, N. Casado, J. Carretero-González, D. Mecerreyes, T. Rojo, *J. Mater. Chem. A* **2017**, *5*, 7137–7143.
- [13] H. Y. Ang, Y. Y. Huang, S. T. Lim, P. Wong, M. Joner, N. Foin, *J. Thorac. Dis.* **2017**, *9*, S923–S934.
- [14] M. J. Heo, C. Lee, S. Y. Choi, Y. M. Choi, I. S. An, S. Bae, S. An, J. H. Jung, *Sci. Rep.* **2020**, *10*, 4493.

Manuscript received: January 28, 2021

Accepted manuscript online: February 10, 2021

Version of record online: March 30, 2021